Article

Relationship Between the Coordination Geometry and Spin Dynamics of Dysprosium(III) Heteroleptic Triple-Decker Complexes

Tetsu Sato [4], Satoshi Matsuzawa [2], Keiichi Katoh [4,*], Brian K. Breedlove [4] and Masahiro Yamashita [1,3,4,*]

1 School of Materials Science and Engineering, Nankai University, Tianjin 300350, China
2 Institute for Materials Research, Tohoku University, 2–1-1 Katahira, Aoba-ku, Sendai 980-8577, Japan; matsuzawa@imr.tohoku.ac.jp
3 Advanced Institute for Materials Research, Tohoku University, 2–1-1 Katahira, Aoba-ku, Sendai 980-8577, Japan
4 Department of Chemistry, Graduate School of Science, Tohoku University, Aramaki-Aza-Aoba, Aoba-ku, Sendai 980-8578, Japan; tetsu.sato.r1@dc.tohoku.ac.jp (T.S.); breedlove@m.tohoku.ac.jp (B.K.B.)
* Correspondence: keiichi.katoh.b3@tohoku.ac.jp (K.K.); yamasita@agnus.chem.tohoku.ac.jp (M.Y.), Tel: +81-22-795-6547 (K.K.), +81-22-795-6544 (M.Y.)

Table of Contents

- ESI-MS data for **1**: **Figure S1, S2** ········ 3, 4
- ESI-MS data for **2**: **Figure S3, S4** ········ 5, 6
- IR spectra for **1** and **2**: **Figure S5** ········ 7
- UV-vis-NIR spectra for **1** and **2**: **Figure S6** ········ 8
- Selected crystallographic data for **1** and **2**: **Table S1** ········ 9
- Selected crystallographic data for **1** and **2**: **Table S2** ········ 10
- PXRD patterns for **1** and **2**: **Figure S7** ········ 11
- Curie-Weiss plots ($1/\chi_M$ versus T) for **1** and **2**: **Figure S8, S9** ········ 12
- Frequency (ν) and temperature (T) dependences of ac magnetic susceptibilities of **1** in a 0 kOe field: **Figure S10** ········ 13
- Frequency (ν) and temperature (T) dependences of ac magnetic susceptibilities of **2** in a 0 kOe field: **Figure S11** ········ 13
- Frequency (ν) and temperature (T) dependences of ac magnetic susceptibilities of **1** in a 1.3 kOe field: **Figure S12** ········ 14
- Frequency (ν) and temperature (T) dependences of ac magnetic susceptibilities of **2** in a 2 kOe field: **Figure S13** ········ 14
- χ_M''/χ_M' versus T (2.5–4 K) plot for **1**: **Figure S14** ········ 15
- χ_M''/χ_M' versus T (2.5–4 K) plot for **2**: **Figure S15** ········ 15
- Extended Debye model: **Eqn. S1–3** ········ 16
- Argand plots (χ_M'' versus χ_M') for **1** at 1.8 K: **Figure S16** ········ 17

- Argand plots (χ_M'' versus χ_M') for **2** at 1.8 K: **Figure S17**······17
- The equationfor Arrhenius plot: **Table S3**······18
- Argand plots (χ_M'' versus χ_M') for **1** in 1.3 kOe: **Figure S18**······19
- Argand plots (χ_M'' versus χ_M') for **2** in 2 kOe: **Figure S19**······19
- The equation for Arrhenius plot: **Table S4**······20

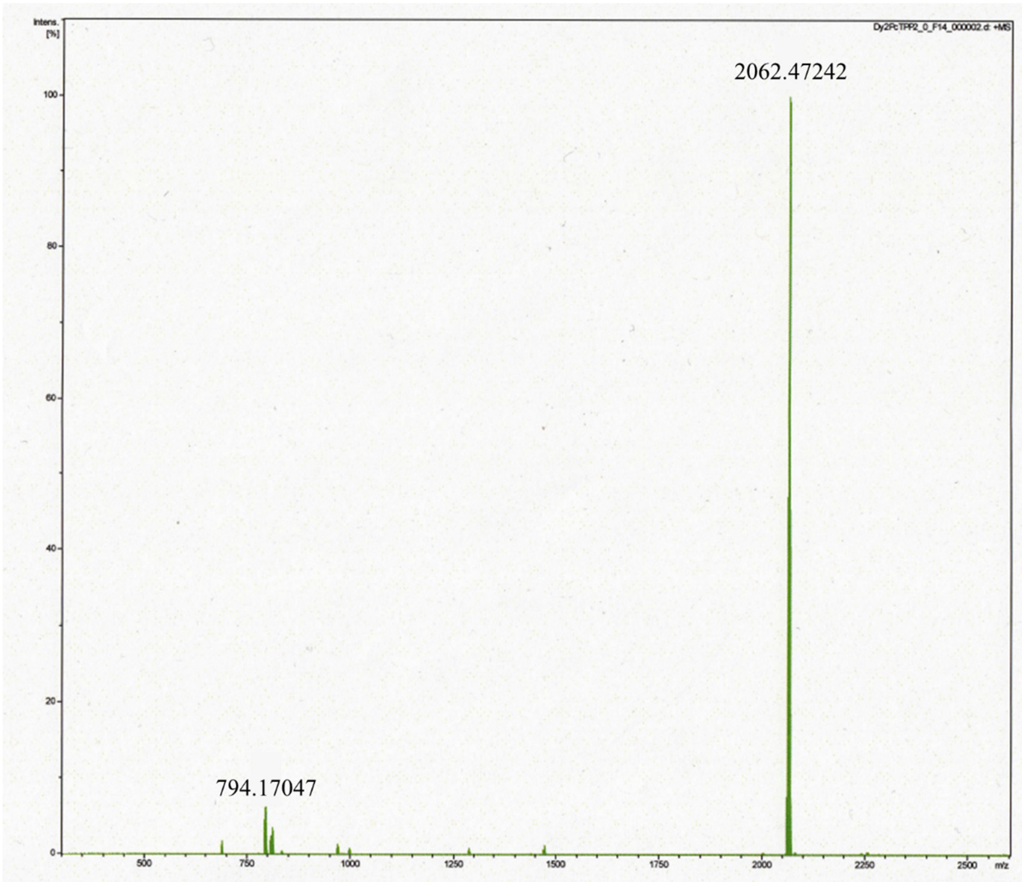

Figure S1. ESI-MS spectrum of **1** in $CHCl_3$. The peak at 2062.47242 corresponds to [M-1^+].

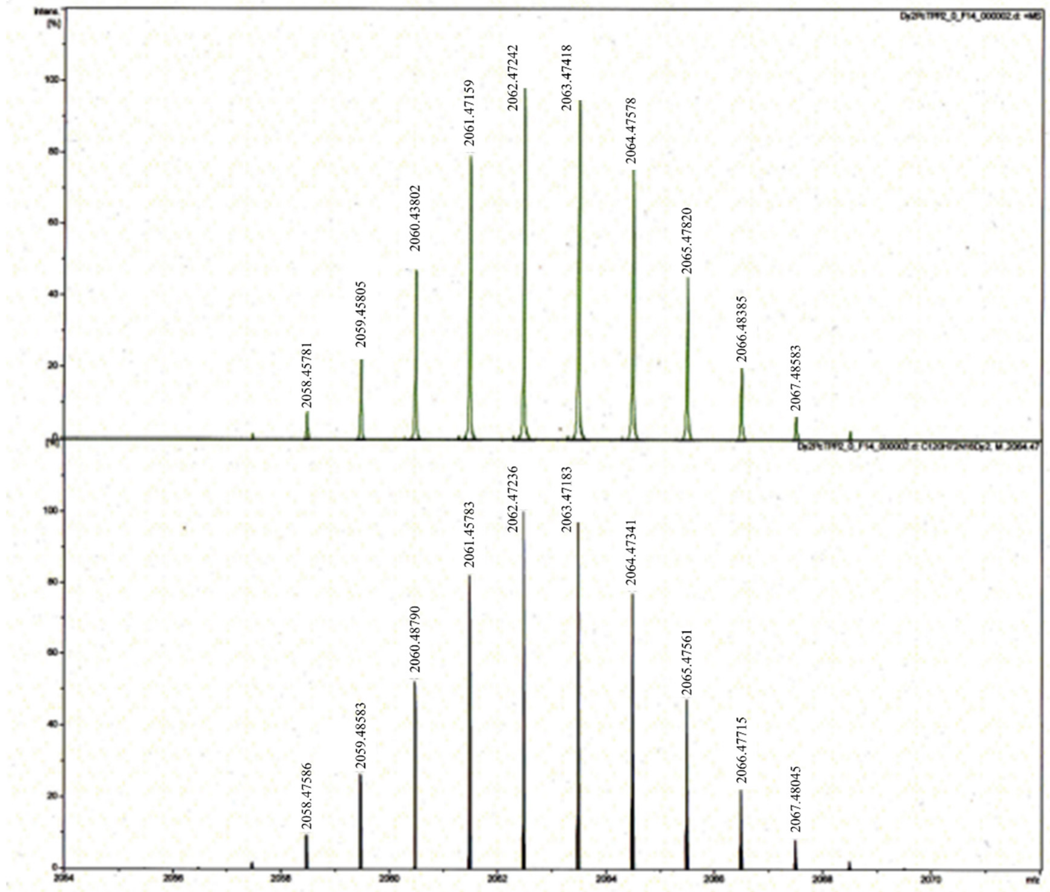

Figure S2. Experimental (top) and simulated (bottom) ESI-MS spectra of **1** in $CHCl_3$. The peak at 2062.47242 corresponds to [M-1$^+$].

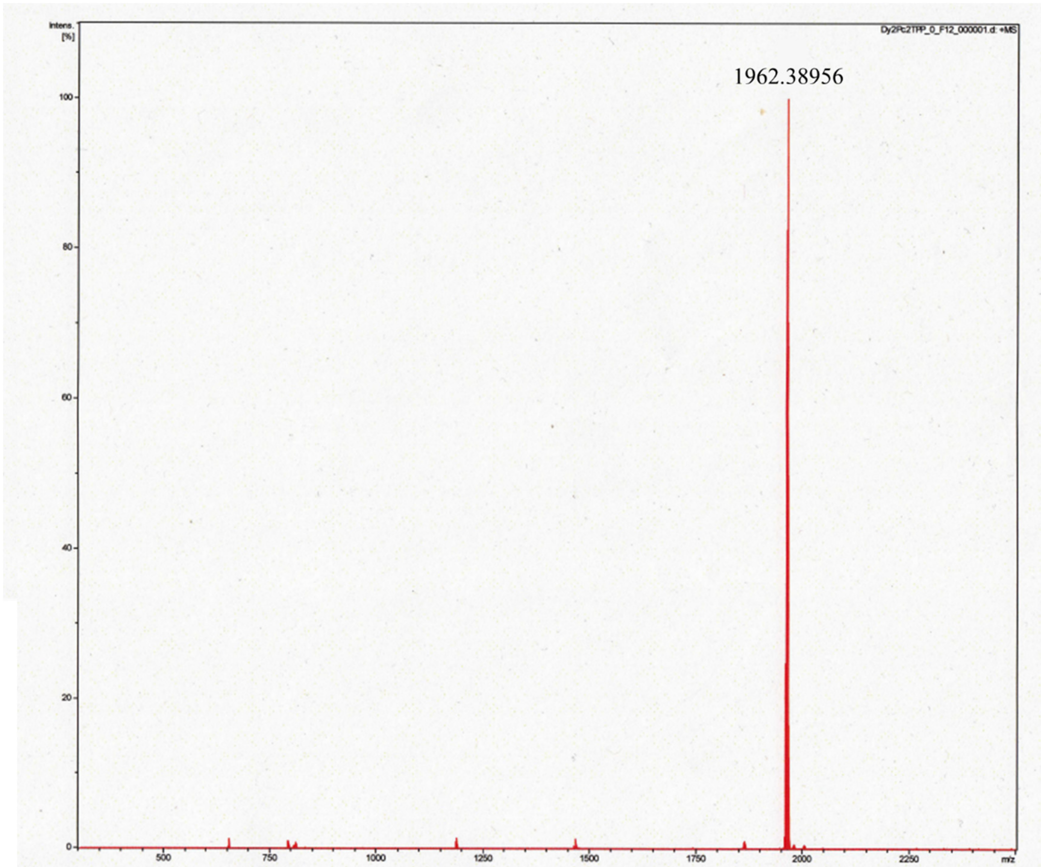

Figure S3. ESI-MS spectrum of **2** in $CHCl_3$. The peak at 1962.38956 corresponds to [M^+].

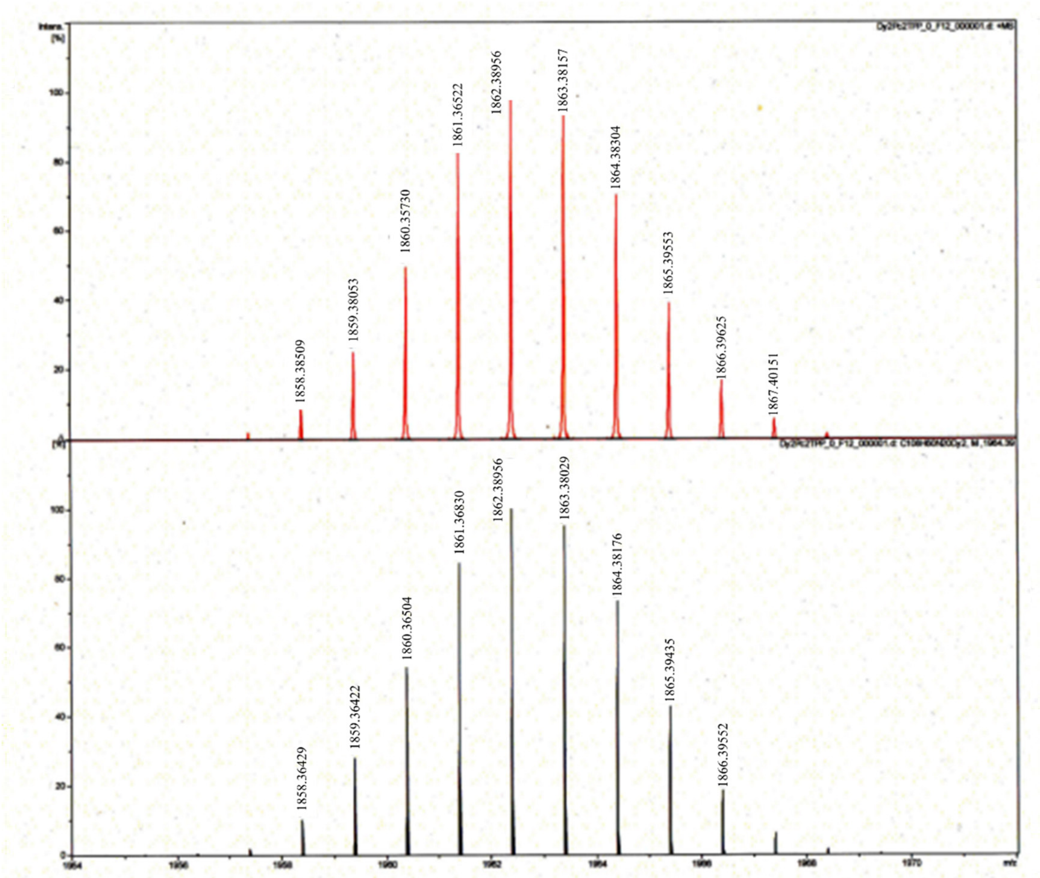

Figure S4. Experimental (top) and simulated (bottom) ESI-MS spectra of **2** in $CHCl_3$. The peak at 1962.38956 corresponds to [M^+].

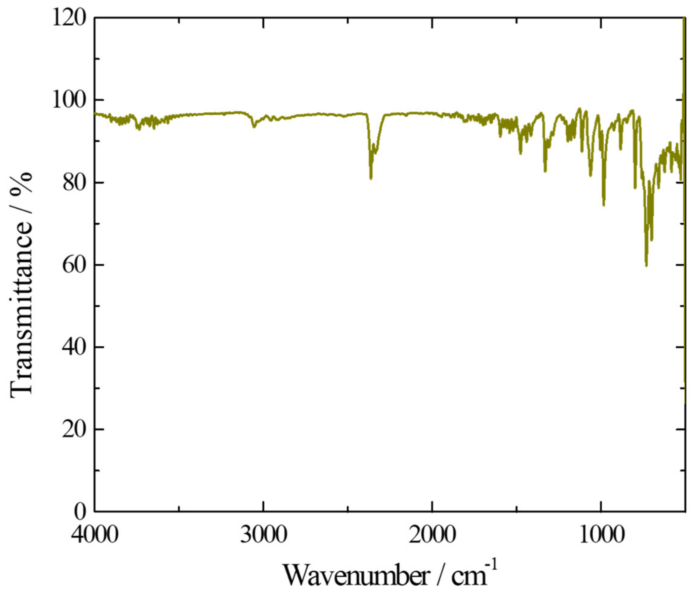

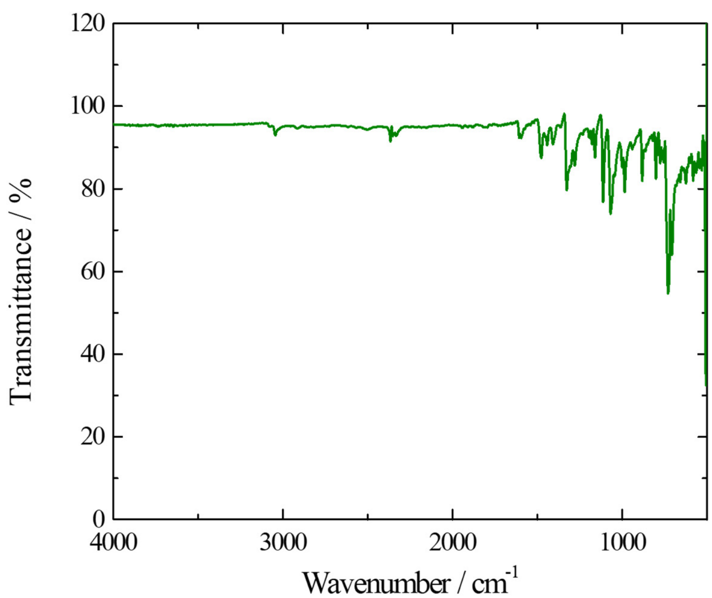

Figure S5. IR spectrum for **1** (top) and **2** (bottom) by using an ATR method at 298 K.

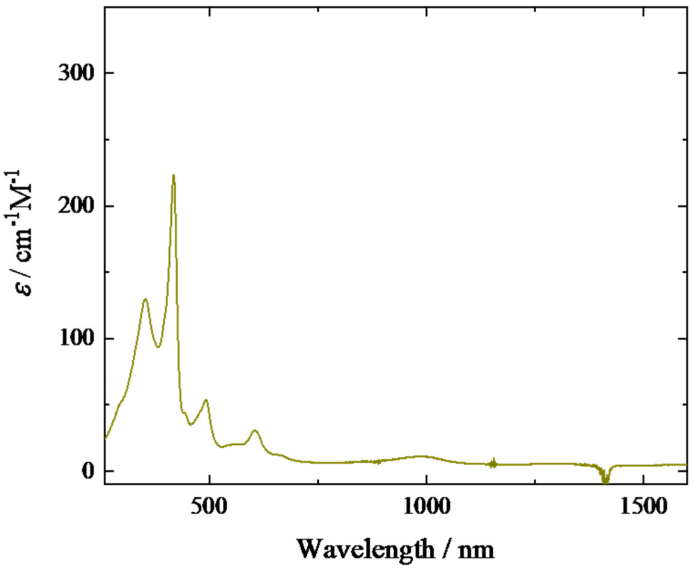

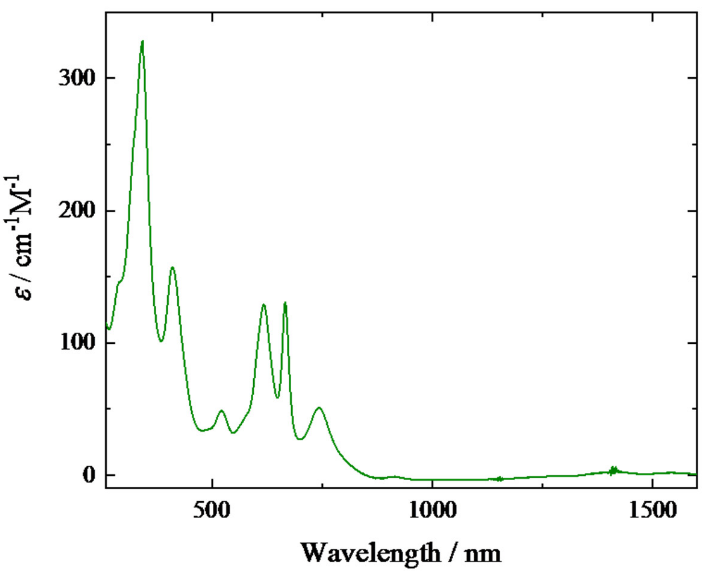

Figure S6. UV-vis-NIR spectra for **1** (top) and **2** (bottom) in $CHCl_3$ (5.1×10^{-3} (**1**), and 4.7×10^{-3} (**2**)) at 298 K.

Table S1. Selected crystallographic data for **1** and **2**

	1	**2**
	$C_{124}H_{72}N_{16}Cl_{12}Dy_2$	$C_{110}H_{62}N_{20}Cl_6Dy_2$
T/ K	100	100
Crystal system	tetragonal	monoclinic
Space group	$I4/m$	$P\ 2_1/c$
a/ Å	14.2765(3)	13.7898(4)
b/ Å	14.2765(3)	27.5804(8)
c/ Å	25.6718(9)	23.5302(7)
α/ deg.	90°	90°
β/ deg.	90°	98.541(3)
γ/ deg.	90°	90°
V/ Å^3	5232.39	8850.0(5)
Z	2	4
$R_1(I > 2s(I))$	0.0346	0.0612
wR_2 (all)	0.0822	0.1254
GOF	1.127	1.032

Table S2. Selected crystallographic data for **1** and **2**

	1	2
1st short contact (Å) (complex and complex)	2.889 (Cl1---H18)	2.817 (C02G---C03B)
1st short contact (Å) (complex and $CHCl_3$)	2.690 (C9---H20)	2.574 (H53---N10)
2nd short contact (Å) (complex and $CHCl_3$)	3.175 (Cl3---H20)	2.891 (Cl03---H9)

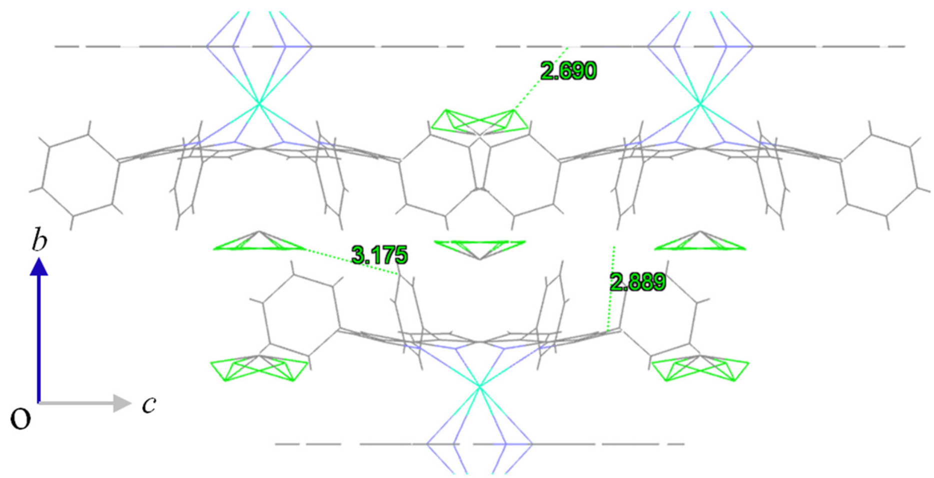

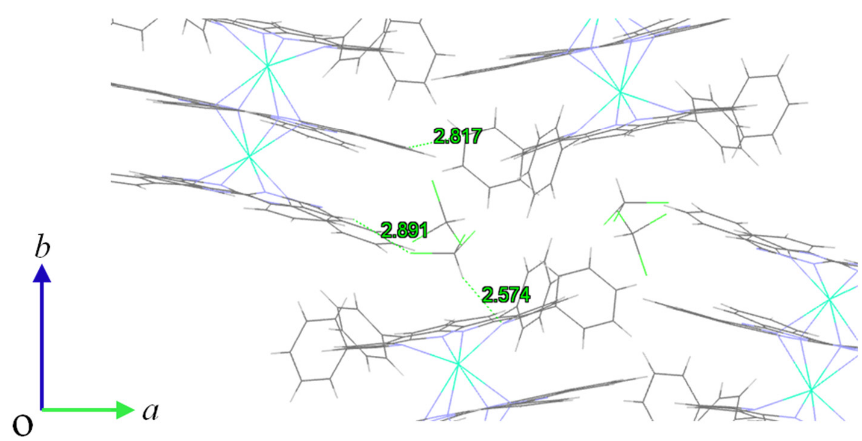

Short contacts in the crystal for **1** (top) and **2** (bottom)

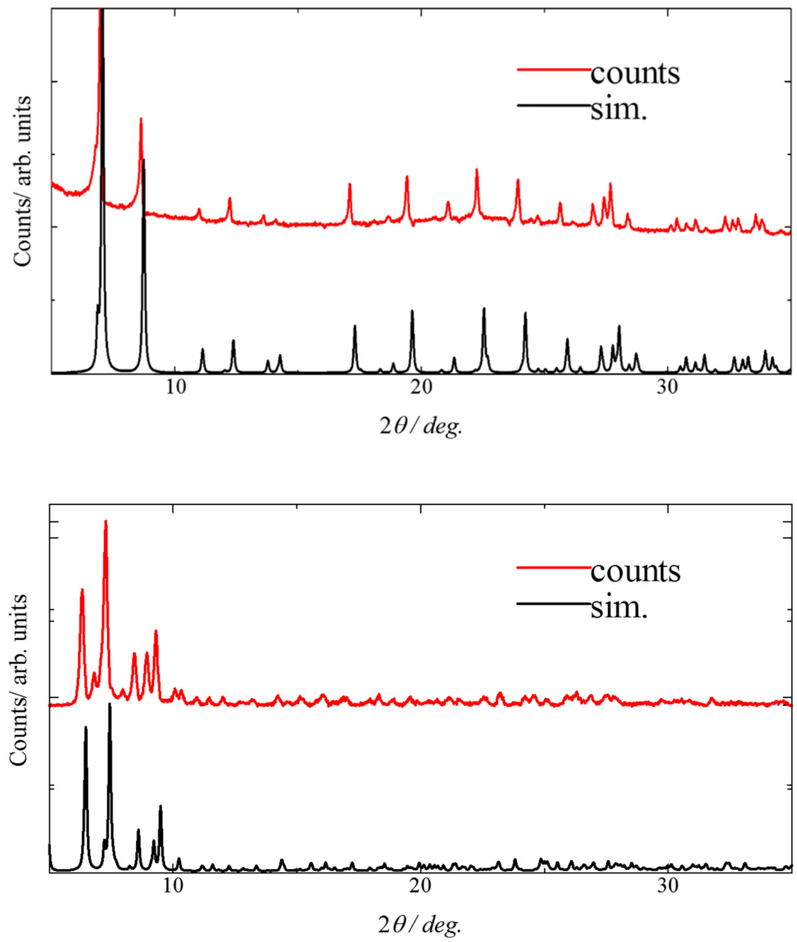

Figure S7. PXRD patterns for **1** (top) and **2** (bottom).

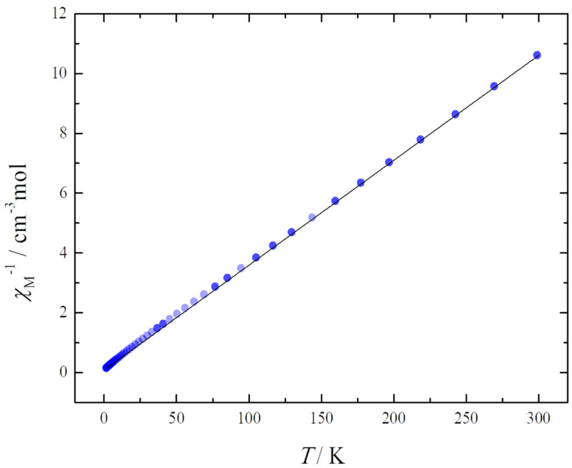

Figure S8. Curie-Weiss plot for **1**. Linear approximation is performed over the entire T range, from which the values of Curie constant (C) (28.50 cm^3 K mol^{-1}) and Weiss constant (θ) (–2.33 K) were obtained.

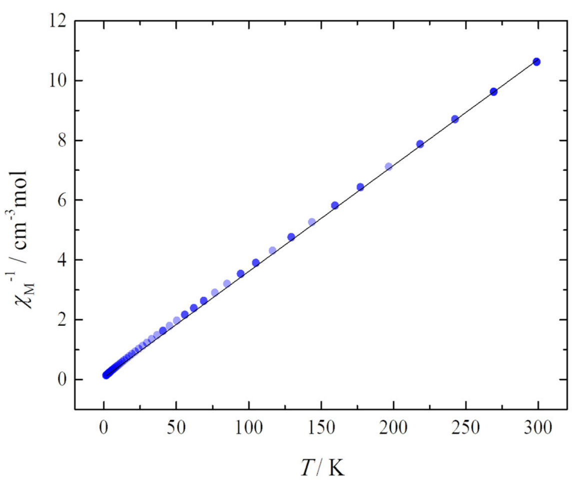

Figure S9. Curie-Weiss plot for **2**. Linear approximation is performed over the entire T range, from which the values of Curie constant (C) (28.20 cm^3 K mol^{-1}) and Weiss constant (θ) (–1.97 K) were obtained.

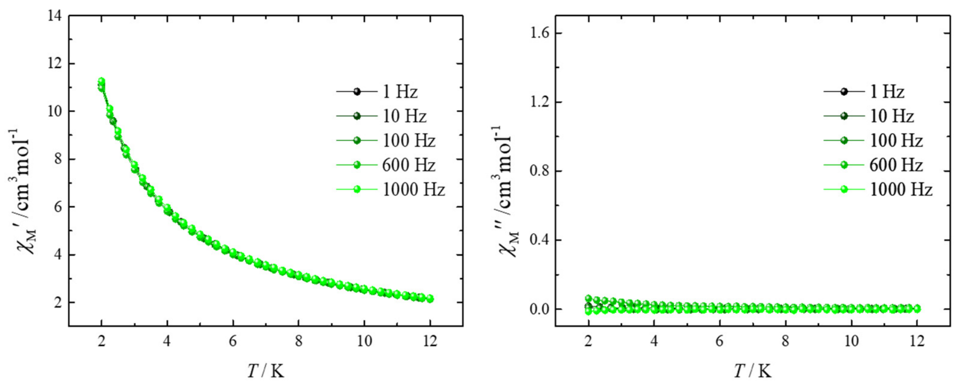

(**a**) (**b**)

Figure S10 Frequency (ν) and temperature (T) dependences of the (**a**) in-phase ($\chi_M{}'$) and (**b**) out-of-phase ($\chi_M{}''$) ac magnetic susceptibilities of **1** in 0 kOe.

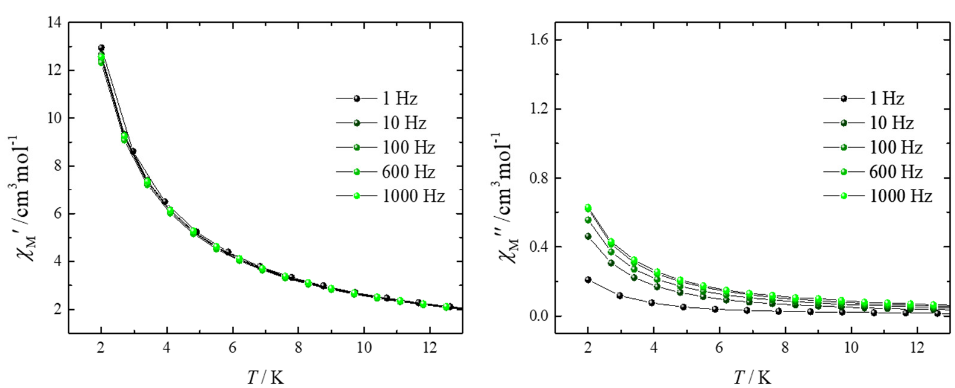

(**a**) (**b**)

Figure S11 Frequency (ν) and temperature (T) dependences of the (**a**) in-phase ($\chi_M{}'$) and (**b**) out-of-phase ($\chi_M{}''$) ac magnetic susceptibilities of **2** in 0 kOe.

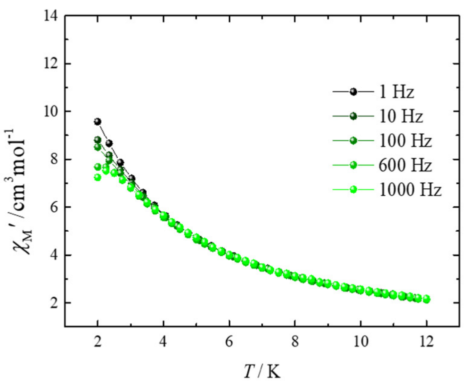

(**a**)

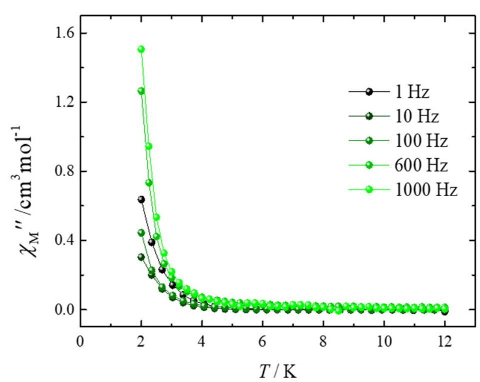

(**b**)

Figure S12 Frequency (ν) and temperature (T) dependences of the (**a**) in-phase (χ_M') and (**b**) out-of-phase (χ_M'') ac magnetic susceptibilities of **1** in 1.3 kOe.

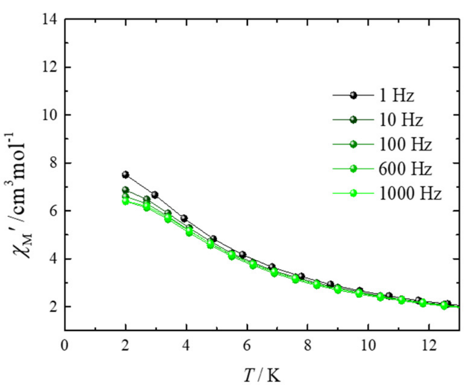

(**a**)

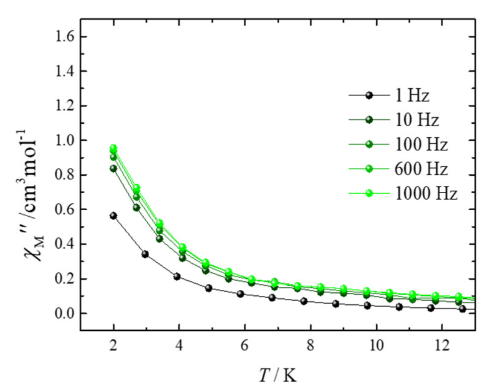

(**b**)

Figure S13 Frequency (ν) and temperature (T) dependences of the (**a**) in-phase (χ_M') and (**b**) out-of-phase (χ_M'') ac magnetic susceptibilities of **2** in 2 kOe.

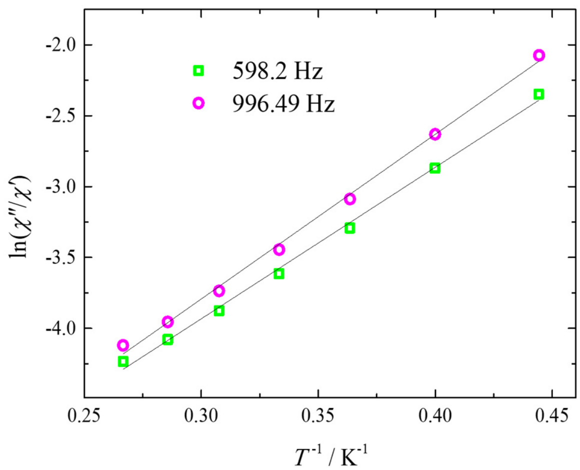

Figure S14 χ_M''/χ_M' versus T (2.5–4 K) plot for **1**

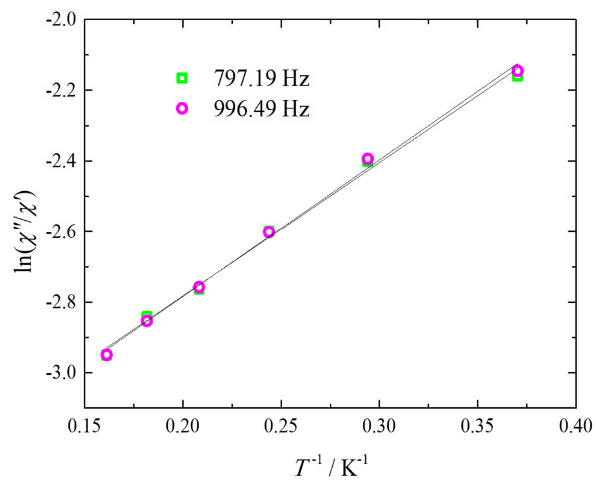

Figure S15 χ_M''/χ_M' versus T (2.5–4 K) plot for **2**

The extended Debye model [1] **(eqn. S1–S3)**

The real (χ_M') and imaginary parts (χ_M'') of the ac magnetic susceptibilities are given by eqns. S2 and S3, respectively.

$$\chi_{\text{total}}(\omega) = \chi_S + (\chi_T - \chi_S)\left[\frac{\beta}{1+(i\omega\tau_1)^{1-\alpha_1}} + \frac{1-\beta}{1+(i\omega\tau_2)^{1-\alpha_2}}\right] \tag{S1}$$

$$\chi'(\omega) = \chi_S + (\chi_T - \chi_S)\left\{\frac{\beta[1+(i\omega\tau_1)^{1-\alpha_1}\sin(\pi\alpha_1/2)]}{1+2(\omega\tau_1)^{1-\alpha_1}\sin(\pi\alpha_1/2)+(\omega\tau_1)^{2-2\alpha_1}} + \frac{(1-\beta)[1+(i\omega\tau_2)^{1-\alpha_2}\sin(\pi\alpha_2/2)]}{1+2(\omega\tau_2)^{1-\alpha_2}\sin(\pi\alpha_2/2)+(\omega\tau_2)^{2-2\alpha_2}}\right\} \tag{S2}$$

$$\chi''(\omega) = (\chi_T - \chi_S)\left[\frac{\beta(\omega\tau_1)^{1-\alpha_1}\cos(\pi\alpha_1/2)}{1+2(\omega\tau_1)^{1-\alpha_1}\sin(\pi\alpha/2)+(\omega\tau_1)^{2-2\alpha_1}} + \frac{(1-\beta)(\omega\tau_2)^{1-\alpha_2}\cos(\pi\alpha_2/2)}{1+2(\omega\tau_2)^{1-\alpha}\sin(\pi\alpha_2/2)+(\omega\tau_2)^{2-2\alpha_2}}\right] \tag{S3}$$

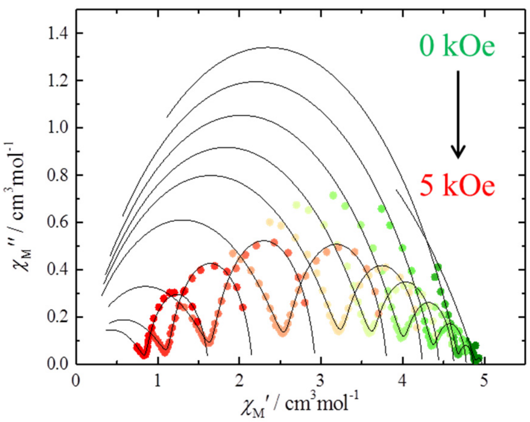

Figure S16. Argand plots (χ_M'' versus χ_M') for **1** at 1.8 K in several dc magnetic fields (0-5 kOe). Black solid lines were guides for eye.

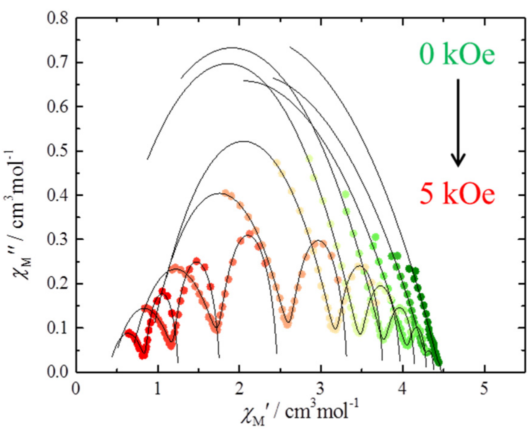

Figure S17. Argand plots (χ_M'' versus χ_M') for **2** at 1.8 K in several dc magnetic fields in the range of 0–5 kOe. Black solid lines were guides for eye.

The equation for fitting the Arrhenius plot

In H/τ plot, the contributions of the spin lattice relaxation and QTM processes were included the following eqn. 1

Table S3. Parameters for fitting the τ verses H plots

	A $[S^{-1}K^{-1}]$	n	B_1	B_2	D $[S^{-1}]$
1 (Low ν)	1.69	0	3.36	0.260	0
1 (High ν)	2.98×10^{3}	2.81	2.84×10^{10}	8.29×10^{6}	0
2 (Low ν)	0	-	3.45	3.90	1.35
2 (High ν)	0	-	0	-	5.97×10^{3}

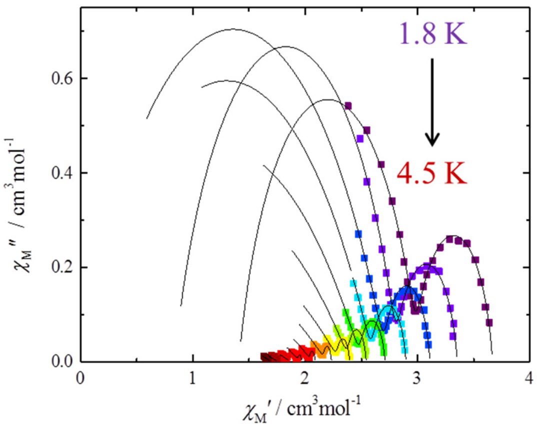

Figure S18. Argand plots (χ_M'' versus χ_M') for **1** in 1.3 kOe in the *T* range of 1.8–4.5 K. Black solid lines are guides for the eye.

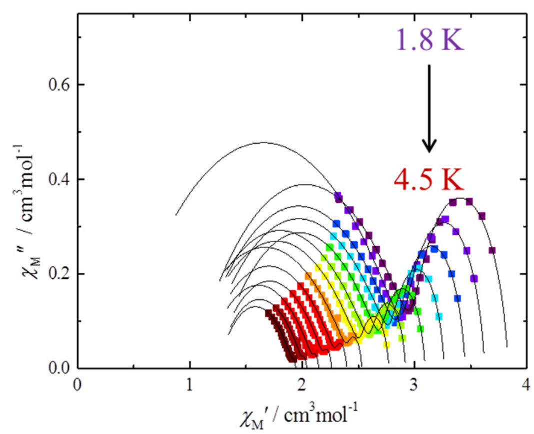

Figure S19. Argand plots (χ_M'' versus χ_M') for **1** in 2 kOe field in the *T* range of 1.8–4.5 K. Black solid lines are guides for the eye.

The equation for Arrhenius plot

In τ verses T plot, contribution of each spin lattice relaxation and QTM process were assigned with following eqn.5

Table S4. Parameters of fitting for τ verses T plot

	A $[S^{-1}K^{-1}]$	n	C $[S^{-1}K^{-m}]$	m	τ_{QTM}^{-1} [s]
1 (Low ν)	0	-	0	-	0.161
1 (High ν)	2.98×10^{3}	2.57	30.6	9	1.77×10^{22}
2 (Low ν)	2.84×10^{10}	1.71	0	-	0
2 (High ν)	0	-	0	-	2.84×10^{10}

References

1. Katoh, K.; Kajiwara, T.; Nakano, M.; Nakazawa, Y.; Wernsdorfer, W.; Ishikawa, N.; Breedlove, B.K.; Yamashita, M. Magnetic relaxation of single-molecule magnets in an external magnetic field: An ising dimer of a terbium(III)-phthalocyaninate triple-decker complex. *Chem. - A Eur. J.* **2011**, *17*, 117–122.
2. Ding, Y.S.; Yu, K.X.; Reta, D.; Ortu, F.; Winpenny, R.E.P.; Zheng, Y.Z.; Chilton, N.F. Field- and temperature-dependent quantum tunnelling of the magnetisation in a large barrier single-molecule magnet. *Nat. Commun.* **2018**, *9*, 1–10.
3. Liu, J.L.; Chen, Y.C.; Tong, M.L. Symmetry strategies for high performance lanthanide-based single-molecule magnets. *Chem. Soc. Rev.* **2018**, *47*, 2431–2453.